

A Generic Computer Model for Amphiphilic Systems

T. Soddemann ^a, B. Dünweg, and K. Kremer

Max Planck Institute for Polymer Research
Ackermannweg 10, D-55128 Mainz, Germany

December 4, 2001

Abstract. We present a simple but versatile off-lattice model for computer simulation studies of amphiphilic systems, constructed mainly for the purpose of computational efficiency. The surfactant molecules are modeled as A–B dimers, where unlike species repel each other, while identical species are also subject to an attraction whose strength drives the various ordering phenomena. This latter potential has been tuned for a good match of interparticle distances, while its short range facilitates fast force calculations. The most important properties of the model are investigated by Molecular Dynamics simulation. In particular, we study the stability of the fluid ordered lamellar phase, as well as the unmixing of the binary fluid of pure A and B.

PACS. 82.70.Uv Surfactants, micellar solutions, vesicles, lamellae, amphiphilic systems – 61.20.Ja Computer simulation of liquid structure – 64.70.Md Transitions in liquid crystals – 64.75.+g Solubility, segregation, and mixing; phase separation – 61.30.Cz Molecular and microscopic models and theories of liquid crystal structure – 61.30.Dk Continuum models and theories of liquid crystal structure

1 Introduction

Amphiphiles are an extremely important class of molecules, offering numerous applications, and showing a very rich physical behavior. In a very broad sense, these molecules can be viewed as being composed of two species (which we shall denote by A and B), whose interactions are such that they would show a strong tendency towards phase separation. This is however prohibited, since the two species are chemically linked. Systems of amphiphiles can form complex morphologies, in order to bring the alike species close to each other. The details of these morphologies depend on the molecular architecture, and on the amount of solvent (i. e. pure A, pure B, or molecules with a high affinity towards either A or B, or non-selective solvent) [1]. In case of symmetric molecules without solvent the typical structure is a lamellar phase where the system organizes in parallel sheets, with the mean molecular axis (the director) perpendicular to the sheets, and alternating (from layer to layer) orientation of the mean $A \rightarrow B$ vector. In the language of liquid crystals, such a phase is referred to as a smectic–A phase. For practical applications, the molecules are particularly important because they enrich at interfaces between A and B or similar molecules, thus drastically reducing the interfacial tension. The most common examples are tensides with a hydrophilic “head” and a hydrophobic “tail”, which can be

used as soaps, and biomembranes composed of lipid bilayers. Another very important class are diblock copolymers, where “head” and “tail” both consist of a large number of monomers. The full phase diagram of these systems has not yet been theoretically explored beyond the mean-field level [1]; this is only one reason why one would like to have a computer model available which mimicks the behavior of these systems. Beyond the equilibrium structure, the systems also show extremely interesting and not fully understood non-equilibrium phenomena, like shear alignment of lamellar structures [2, 3], the formation of “onion” structures [4], or “cascade nucleation” of A droplets in a B phase shielded by amphiphiles under the influence of continuous driving [5–7]. For investigations concerning the fundamental mechanisms in these phenomena, atomistic models are computationally too expensive, and also not needed, since the basic physics is identical. For many questions it is even unimportant to distinguish between low-molecular weight tensides or lipids and block copolymers. Although atomistic simulations can nowadays reach quite impressive length and time scales [8], it is nevertheless clear that phenomena like shear alignment [2, 3], which happen on hydrodynamic length and time scales, and require large systems, are out of reach. For this reason, there has been a long tradition of computer simulations of models which coarse-grain the underlying chemistry. Depending on the question under consideration, different levels of chemical detail are needed. While “united atom” approaches [9] still attempt to catch most chemical features, other models keep only the most salient features,

^a present address: Johns Hopkins University, Department of Physics and Astronomy, 3400 North Charles Street, Baltimore, MD 21218, USA

i. e. the tendency to unmix, the connectivity, and sometimes a sketchy representation of the molecular architecture (for example a large asymmetry in the size of “head” and “tail”). This reduction in the number of degrees of freedom yields a tremendous computational speedup; in our work with polymer models we found factors of 10^4 or even more [10]. For a long time, lattice models [11,12] have been very popular. However, we strongly believe that with nowadays’ computers featuring fast floating point arithmetics, a continuum model offers practically the same computational efficiency, while at the same time being able to much more easily implement complex physical situations like shear flow, and avoid lattice artifacts (like unphysically large bending of lamellar sheets, incompatibility of the natural layer spacing with the lattice constant, no continuous rotation of molecules, etc.). The most logical choice are, in essence, standard Lennard–Jones particles connected by springs, and suitably chosen interactions to distinguish A and B. Compared to the “united atom” approach [9], substantial amounts of CPU time can be saved by avoiding the complicated bond–bending terms. Such models have already successfully been implemented before [13–16], and simulations on rather large scales have been performed [16]. Nevertheless, within the class of these models there is still opportunity for further optimization, which so far has apparently not been exploited. It is the purpose of the present paper to fill this gap. The model which we wish to outline here is in spirit very similar to that of Ref. [16]; however, there are some small but important differences. Firstly, we limit the interaction range to only the nearest–neighbor shell, such that the number of force calculations is reduced substantially. Secondly, we use a more efficient thermostat, which allows us to use a time step about twice as large. We estimate that these two improvements make our simulations roughly one order of magnitude faster. Thirdly, we use the strength of the attractive interaction as the temperature–like parameter, while keeping the average kinetic energy and the curvature of the potentials constant. This is optimal for Molecular Dynamics, allowing us to use the same large time step throughout in the phase diagram. In the present paper, we wish to outline the simplest prototypic version of such models, and test its behavior (in particular, phase behavior) in simple equilibrium situations where the expected physics is clear. Extensions to more complicated versions, which mimic the underlying chemistry in a slightly more detailed way [17], and applications to nontrivial physical situations, like simulations of shear alignment [18], are left for future publications.

The paper is organized as follows: In Sec. 2 we outline the reasoning and some of the test runs which have lead us to the final formulation of our model. In Sec. 3 we describe the most important properties of the system as obtained by simulations, in particular its phase behavior, demonstrating that it is indeed useful for the desired purpose. Finally, we conclude in Sec. 4.

2 Development of the Model

2.1 Interactions

The basic ingredients of our model are particles which interact through spherically symmetric potentials. These potentials should be continuous, in order to facilitate a standard Molecular Dynamics procedure like the Verlet algorithm [19], and short–ranged, in order to keep the number of force calculations at a minimum. A convenient choice for this is a Lennard–Jones (LJ) potential that is truncated at the minimum, and shifted:

$$U_{LJ} = \begin{cases} 4\epsilon \left[\left(\frac{\sigma}{r}\right)^{12} - \left(\frac{\sigma}{r}\right)^6 + \frac{1}{4} \right] & r \leq 2^{1/6}\sigma \\ 0 & r \geq 2^{1/6}\sigma \end{cases} \quad (1)$$

This potential has found widespread applications for the simulation of bead–spring models for polymers [20,21]. Here, ϵ sets the energy scale and σ the length scale. We will henceforth use Lennard–Jones units where $\epsilon = \sigma = 1$; the mass m of the particles is also set to unity, such that time is measured in units of $\tau = (\sigma^2 m / \epsilon)^{1/2}$. A typical dense system is characterized by a particle density of $\rho = 0.85$, and temperature $k_B T = 1$. This dense repulsive Lennard–Jones fluid will be the reference system from which we construct our model. The pair correlation function (PCF) $g(r)$, i. e. the normalized density–density correlation function, with $g(r) \rightarrow 1$ for $r \rightarrow \infty$, is shown in Fig. 1 for this LJ fluid.

As a minimal model for amphiphilic molecules, we just consider dimers of different species. From the polymer simulations it is known that it is computationally efficient to link the dimers via anharmonic FENE (“finitely extensible nonlinear elastic”) springs with spring constant k and maximum extension R_0 :

$$U_{FENE} = \begin{cases} -\frac{1}{2}kR_0^2 \ln \left[1 - \left(\frac{r}{R_0}\right)^2 \right] & r < R_0 \\ \infty & r \geq R_0 \end{cases} \quad (2)$$

While for the polymer simulations usually the values $k = 30$ and $R_0 = 1.5$ are used [20], we here use a somewhat weaker attraction, $k = 5$, $R_0 = 2$. The reason is that we wish to adjust the typical bond length to the typical interparticle distance in the dense Lennard–Jones fluid (rather close to $2^{1/6}$, see Fig. 1). By this match we make sure that the model will also allow for an ensemble where the connectivity is not fixed, but the bonds are created and deleted between monomers. If the length scales would not fit, attempts of such processes would much too frequently be rejected [17]. Another important aspect of using an increased bond length is the enlarged softness of a layer with respect to shear: The longer the bonds are, the more freedom they have to be tilted with respect to the layer normal, while still avoiding strong intra–layer contacts between unlike species.

Furthermore, the model needs to include different interactions between A and B particles, in order to distinguish them and drive the tendency towards phase separation.

The simplest model has identical interactions for A–A and for B–B contacts, while an A–B contact is more repulsive, or less attractive, and thus unfavorable. Ideally, one would like to do this via repulsive potentials only, for example by increasing the prefactor in Eq. 1 for A–B contacts, the advantage being twofold: Firstly, one would stick to a very short interaction range, and thus to few force calculations, and secondly the system would not exhibit a gas–liquid transition, which is not of interest per se, and would only introduce an unwanted complication into the system. Actually, this approach has been very successful to model the phase separation of polymer blends, and the microphase separation of block copolymers [22]. In that case, however, a very small difference in the interaction is already sufficient to drive the phase transition, as the polymerization strongly reduces the translational entropy, resulting in $T_c \propto N$, where T_c is the critical temperature, and N the degree of polymerization. Conversely, our low–molecular weight system would need a quite strong repulsion between A and B in order to access phase separation. Note that it is computationally more efficient to vary the interaction strength to drive the phase transition, rather than the temperature — the potentials are optimized such that the Molecular Dynamics, with its interplay between potential energy and kinetic energy, runs best for $k_B T = 1$. Tests have then shown that actually a very strong repulsion would be needed, requiring a very small time step, which again is inefficient. For this reason, we have resorted to the second choice, and included an attractive tail between the A–A pairs and the B–B pairs, while the A–B contacts are just subject to the purely repulsive Lennard–Jones potential.

For the choice of the attractive tail, the following considerations for this first version of our model are important: (i) In the general spirit of a minimal model, we want to avoid the presence of several molecular length scales, which might lead to competition, frustration, etc. So we want that the typical interparticle distance is the same for A–A, B–B, and A–B bonds. In other words: The additional attractive tail should not substantially distort the pair correlation function $g(r)$ of the original repulsive Lennard–Jones fluid, at least with respect to the positions of the maxima and minima. Guided by the same idea, we had already adjusted the parameters of the bond potential, Eq. 2. (ii) The tail should be rather short–ranged, for reasons of efficiency. (iii) In order to avoid instabilities in Molecular Dynamics simulations, the potential should be continuous, and have continuous first derivatives.

For these reasons, the potential should remain unchanged for $0 < r < 2^{1/6}$, while the attractive tail should reach from $r = 2^{1/6}$ to the first minimum of $g(r)$ (which occurs roughly at $r = 1.5$, as seen from Fig. 1), such that only the first neighbor shell is included in the interaction. Such a potential will then of course allow for a gas–liquid transition, and, as a potential complication, favor crystallization into an fcc structure, since any frustration effects between length scales have been deliberately avoided. These issues will be considered in the next section in more detail. The tail should thus have zero derivative

at $r = 2^{1/6}$ and at $r = 1.5$, while it should have the values zero at $r = 1.5$, and $-\phi$ at $r = 2^{1/6}$, where ϕ is the depth of the attractive part, and is used by us as the independent parameter by which we drive the system into the ordered phase. Using a shifted cosine wave in r^2 , one thus obtains

$$U_{LJcos} = \begin{cases} 4 \left[\left(\frac{1}{r} \right)^{12} - \left(\frac{1}{r} \right)^6 + \frac{1}{4} \right] - \phi & r \leq 2^{1/6} \\ \frac{1}{2} \phi [\cos(\alpha r^2 + \beta) - 1] & 2^{1/6} \leq r \leq 1.5 \\ 0 & r \geq 1.5 \end{cases}, \quad (3)$$

where α and β are determined as the solutions of the linear set of equations

$$2^{1/3} \alpha + \beta = \pi \quad (4)$$

$$2.25 \alpha + \beta = 2\pi, \quad (5)$$

i. e. $\alpha = 3.1730728678$ and $\beta = -0.85622864544$.

As an alternative, we also tried a third–order polynomial in r^2 ,

$$U_p/\phi = A + r^2(B + r^2(C + r^2D)), \quad (6)$$

where the same requirements yield $A = 7.979574673$, $B = -17.52538691$, $C = 10.84948485$, $D = -2.060727237$. However, in benchmarks we found that this potential is only a few percent faster than the cosine version, the reason being that the trigonometric functions are implemented as fast hardware instructions on the processors we used (Compaq Alpha EV5, EV56, EV6, EV67, and Intel Pentium II and III). We therefore kept the original version, Eq. 3. All results that follow will exclusively refer to this potential.

Figure 1 shows the resulting $g(r)$ of a monomer fluid of $N = 10000$ particles who are all subject to U_{LJcos} . While $\phi = 0$ is the original repulsive Lennard–Jones fluid, the amplitude is systematically increasing with ϕ . However, the position of the maxima and minima is nearly unchanged, as desired. $\phi = 2.0$ is close to the fluid–solid transition (see below).

Figure 2 compares $g(r)$ to the bond lengths which result from the FENE potential, Eq. 2, at a typical state point $\phi = 1.5$. It is seen that also these lengths match quite nicely.

2.2 Computational Details

The simulation method we apply is Molecular Dynamics (MD). For the basics of MD we refer the reader to Refs. [19, 23]. For stabilization purposes, we use a Langevin thermostat [24]. The equations of motion are given by

$$m \ddot{\mathbf{r}}_i = -\nabla_i U - \Gamma \dot{\mathbf{r}}_i + \mathbf{W}_i(t) \quad (7)$$

where the friction coefficient Γ and the strength of the random noise $\mathbf{W}_i(t)$ are related via the fluctuation dissipation theorem:

$$\langle \mathbf{W}_i(t) \cdot \mathbf{W}_j(t') \rangle = 6k_B T \Gamma \delta_{ij} \delta(t - t'). \quad (8)$$

U denotes the sum over all interactions of the bead i , and the temperature is always fixed at the value $k_B T = 1.0$. The equations of motion are integrated by using a velocity Verlet updating scheme [19]. The simulations were carried out in the constant volume (NVT) as well as in the constant pressure (NPT) ensemble. For the NPT ensemble simulation a modified velocity Verlet algorithm was used, and the “box” degree of freedom coupled to a Langevin heat bath as well [25]. The time step used in the simulation was $\Delta t = 0.01$. The friction constant is set to the small value $\Gamma = 0.5$, thus ensuring that our dynamics is not too far away from the Hamiltonian limit. For a reasonable choice of parameters for the NPT ensemble, see Ref. [25]. The simulation box was always cubic with periodic boundary conditions. We used a highly optimized domain decomposition scheme in order to run the simulations in parallel on a Cray T3E. For more details of this algorithm, we refer the reader to Ref. [26].

Figure 3 shows that indeed the strategy of confining the interaction range to the first neighbor shell pays off in terms of computational efficiency: While the purely repulsive system is clearly by far the fastest, we only lose a factor of two in speed when increasing the interaction range to 1.5. If we would have used the “canonical” interaction range 2.5, then the loss would rather be a factor of eight. Although modern computers are fairly fast, this speedup is nevertheless of importance for the large system sizes which are needed to study, for example, non-equilibrium phenomena in shear flow.

We also augmented our algorithm by Monte Carlo (MC) moves. Firstly, in order to study the unmixing of unlike monomers (just a binary fluid, with no connectivity potential), we used a semi-grandcanonical ensemble where the total number of particles is fixed, while the fraction of A (or B) particles is allowed to fluctuate, such that the chemical potential difference $\Delta\mu$ is being held fixed. For symmetry reasons, the unmixing occurs at $\Delta\mu = 0$. The fluctuations in composition are then facilitated via stochastic “flips”, which can change an A particle to a B particle, or vice versa [22]. This was implemented via a simple single spin flip algorithm using the standard Metropolis [27] criterion.

Secondly, one might also think about the analogous procedure for a system of dimers: An A-B dimer is “flipped” to a B-A dimer, or vice versa. Such a scheme would certainly somewhat speed up the equilibration when a lamellar structure is formed. Nevertheless, we have not implemented these moves, since they would have required substantial communication in our parallel program. Its data structure builds directly on that of Ref. [26], where the elementary units are the monomers, such that a dimer can be crossing processor boundaries. Furthermore, one should note that these dimer flips are far less important than the spin flips in the binary fluid: An unmixing system without the MC procedure would exhibit a conserved order parameter and hence “hydrodynamic slowing down”, i. e. the necessity of transport over macroscopic distances. Conversely, in the case of the formation of a lamellar structure, the order parameter is not con-

served, such that only local rearrangements are necessary. A fully grand-canonical scheme, in which the concentration of each species, including the amphiphiles, is controlled via chemical potentials, is currently being developed [17]. This approach is expected to be very useful for binary and ternary systems of solvent(s) and amphiphiles.

3 Simulation Results

3.1 Identical Monomers

The simplest system to study consists of identical monomers only. Figure 4 gives a rough sketch of the expected phase diagram in the (ϕ, P) -plane, P denoting the pressure. Both a gas-liquid transition as well as a fluid-solid transition are expected, although the gas-liquid transition must not necessarily occur [28]. Since we are mainly interested in the behavior at densities near the typical value $\rho = 0.85$, we have not attempted to answer this question and map out the phase diagram as a whole. We rather restricted ourselves to varying ϕ at constant pressure $P = 1.0$; previous test runs had shown that this is a typical pressure for a dimer system at the typical high density near the order-disorder transition (ODT), see below. Our results indicate that along this chosen path only a fluid-solid transition occurs.

This transition was located by obtaining a hysteresis loop of the density as a function of ϕ , for a system of $N = 10000$ particles; this large system size was necessary in order to obtain good accuracy in the metastable states. We started in the fluid phase and increased ϕ systematically, until a jump in the density was observed, after which we swept back. The final configuration of the previous run was always used as initial configuration for the next ϕ value; the data were always taken over sufficiently short runs such that no jumping back and forth between the co-existing phases was observed. Figure 5 shows the resulting hysteresis loop. We did not attempt to locate the fluid-solid transition very accurately (this would have required thermodynamic integration or finite-size scaling [29]), but it is quite clear that it occurs for $1.4 < \phi < 1.8$. Therefore, the simulations of the amphiphilic systems should clearly avoid such large ϕ values.

The solid phase is further characterized by a strongly reduced diffusion. Figure 6 shows the mean square displacement (MSD) of a single particle as a function of time for different ϕ values along the path we had studied. To this end we simulated an $N = 500$ particle system in the NVT ensemble, starting off from the final configurations of the corresponding NPT run. The diffusion constant is extracted from the long-time behavior via the Einstein relation in d spatial dimensions (here $d = 3$)

$$D = \lim_{t \rightarrow \infty} \frac{1}{2t} \langle (\mathbf{r}(t) - \mathbf{r}(0))^2 \rangle, \quad (9)$$

resulting in the values given in Table 1. Note that the mean square displacement has to be measured in the center-of-mass reference frame of the overall system,

which diffuses as well. While diffusive behavior is observed without any problems in the fluid phase, it turns out that at the state point in the solid phase ($\phi = 2.4$) the mobility is actually so small that we were unable to observe the leaving of the local “cage” on the time scale of our simulation; hence we are only able to give an upper bound for the diffusion constant there. Moreover, it should be noted that the data for $\phi = 1.9$ correspond to a metastable fluid; the run which produced these data was substantially shorter than the corresponding run for Fig. 5, such that the system did not have enough time to go into the solid phase.

Details of the crystal structure are revealed by the static structure factor $S(q)$, which we show in Fig. 7 for $\phi = 2.4$ in comparison to $\phi = 1.4, 1.8, 2.0$ in the liquid state for an $N = 10000$ system along the path studied. One clearly sees a much more pronounced structure with long-range order. The position of the peaks is compatible with an fcc crystal [30]. Moreover, a determination of the number of nearest neighbors via integration over the first peak of $g(r)$ yields the value 12, as expected for the fcc structure. $\phi = 2.0$ is still a metastable liquid (again, these data were taken from a much shorter run than those for Fig. 5), as seen from the density. Here the first maximum of $S(q)$ has a value of roughly 3.5, clearly above 2.8, which, according to the empirical Hansen–Verlet criterion [31], should mark the onset of crystallization.

3.2 Binary Mixture

For a system which contains rather two different species A and B, the phase behavior becomes more complicated, since at large values of ϕ the two species will unmix (macrophase separation, MPS). The qualitative phase diagram which we expect is drawn in Fig. 8. We have studied MPS in the semi-grandcanonical ensemble for a system at fixed density $\rho = 0.85$ as a function of ϕ . This situation is qualitatively depicted in Fig. 9. It is particularly important to know if the MPS occurs for smaller ϕ than crystallization — otherwise no fluid phase in the unmixed state would exist, and it would be quite unlikely that a dimer system exhibits a fluid lamellar phase.

The order parameter is given by $m = N_A - N_B$ and can vary from $-N$ to $+N$. According to the usual theory of finite-size scaling [29], the standard cumulant ratio $1 - \langle m^4 \rangle / (3 \langle m^2 \rangle^2)$, plotted as a function of ϕ for different system sizes, should intersect at one point which is a very good estimate for ϕ_c . Since actually the value of the ratio at the intersection point is known (it depends only on the universality class and assumes the value 0.47 for the case of three-dimensional Ising-like critical behavior [32]), we have only studied a single system size $N = 4000$, with a very long run. The resulting cumulant ratio is plotted in Fig. 10, from which we can roughly estimate $\phi_c = 0.65$, which is fortunately far below the fluid–solid transition. One should expect that the ODT for a dimer system will occur at a somewhat higher ϕ value. The reason is rather simple: Compared to the formation of a lamellar phase, unmixing is much more efficient in removing internal interfaces. Therefore the ODT has a weaker driving force

and hence needs a stronger coupling. For this reason, it must be checked if the ODT occurs before crystallization.

3.3 Dimeric Systems

A system of A–B dimers allows for three independent order parameters within the liquid phase. First of all, the molecules can orient along a spontaneously selected axis (the director), without distinguishing between A and B. If no additional ordering would occur, then such a phase would be nematic. Nematic ordering is measured via the symmetric and traceless Saupe tensor [33]

$$Q_{ij} = \frac{3}{2} \left(\hat{r}_i \hat{r}_j - \frac{1}{3} \delta_{ij} \right), \quad (10)$$

where i and j are Cartesian indices, δ_{ij} is the Kronecker symbol, and \hat{r} denotes a unit vector along the molecular axis. In the isotropic phase the volume average (or ensemble average) of Q_{ij} is identically zero, while in the uniaxial nematic phase Q_{ij} has the three eigenvalues $(S, -S/2, -S/2)$, where $S > 0$ is the nematic order parameter, which at most can assume the value $S = 1$ corresponding to the perfectly ordered state. In our simulation, we measured, at any particular time, the volume average of Q_{ij} and determined the largest eigenvalue. The time average of these defines the numerical estimate for S .

Furthermore, there can be breaking of translational invariance and the formation of a smectic phase. In a smectic–A phase, the sheets are perpendicular to the director. This can be measured by studying the density–density correlation function (or the structure factor) along the director, where it exhibits quasi long-range order [34], and perpendicular to it, where the structure is fluid-like.

Finally, there can also be an orientation of the A–B molecules along the director axis \hat{n} : The vector from A to B can either point with identical probabilities in the direction $+\hat{n}$ and $-\hat{n}$ (disordered state), or prefer one particular direction (ordered state).

For our system, there are only two fluid phases present: The disordered phase, where all order parameters vanish, and the lamellar phase, in which all three order parameters are nonzero. Further fluid phases, which are theoretically possible (i. e. not prohibited by fundamental symmetry arguments), like a disordered smectic or nematic phase, or an oriented nematic phase, are not expected for our system, and they have not been observed. The expected qualitative phase diagram is thus shown in Fig. 11, where we also show the path along which we have studied the order–disorder transition at constant volume and constant number of dimers.

It is clear that the ODT must be of first order, since already nematic ordering enforces first-order behavior, as is known from symmetry analysis and Landau–deGennes theory [33]. There is thus a slight problem with studying the ODT in the constant-volume ensemble: Strictly spoken, one must expect that the isotropic and lamellar

phases have different densities at coexistence, and therefore phase separation (i. e. unmixing of the isotropic and the lamellar phase) must occur. However, it is expected that the density difference is so small that the phases will not unmix unless the system is extremely large: For a small system, the free energy penalty of introducing an interface into the system will outweigh the bulk free energy gain obtained from phase separation. Indeed, we checked that both coexisting phases, which we found via hysteresis loops for S (see below), have roughly the same pressure at the same state point. This shows that the approach is consistent within our numerical resolution. For high-accuracy studies however, this issue must be kept in mind. The constant-pressure ensemble was not used since it is computationally more expensive and less easy to handle.

Another criticism against the constant-volume ensemble is the incompatibility of the linear box size L with the smectic layer spacing d . However, when the system becomes large, then this distortion becomes small. Furthermore, one has to take into account that the layers can rotate with respect to the box, and this allows for non-integer ratios L/d : The periodic boundary conditions enforce that there must be integers m_x , m_y , and m_z such that the layer spacing in x direction is L/m_x (for the y and z directions analogously). If the origin of the coordinate system is in the first layer, then the second layer is given by $\hat{n} \cdot \mathbf{r} = d$, where \hat{n} is the director unit vector. This equation must therefore hold specifically for $\mathbf{r} = (L/m_x, 0, 0)$, and thus $\hat{n}_x = (d/L)m_x$ (for y and z analogously). Normalization of \hat{n} thus implies $L/d = \sqrt{m_x^2 + m_y^2 + m_z^2}$, i. e. any ratio that can be represented in this form is permitted, and the system will choose the numbers m_x , m_y and m_z to minimize the deviation from the optimum layer spacing.

For Fig. 12, which shows a typical configuration deep in the lamellar phase, we first had measured the sheet thickness and then adjusted the system size in order to fit the sheets nicely (L/d integer). We therefore study a system not of 100000 monomers, but rather $N = \rho d^3 (L/d)^3 = 97336$. One easily obtains a nice lamellar phase which extends over the whole sample if the simulation is started in an ordered state. Such a configuration is shown in the left part. Conversely, if the system is quenched from the disordered state, the system first develops a multi-domain structure, as shown in the right part. Such a configuration then relaxes very slowly into the true equilibrium state, by annealing the domain walls. Figure 13 shows the hysteresis loop in the nematic order parameter S for this system. Each state point was observed for 2000 LJ time units; the branch in the ordered phase was obtained by simulating a system which was originally prepared in a perfectly ordered state. The data corresponding to the disordered branch at intermediate S values correspond to time averages over the slow relaxation process of domain annealing and are hence not true equilibrium averages. The ODT is thus localized at roughly $\phi = 1.2$. This result coincides with a simulation of a smaller system $N = 10000$ which was run under constant pressure conditions $P = 1.0$ (stars and boxes in Fig. 13).

The important point is that the ODT occurs at a smaller ϕ value than what we found previously for crystallization of the monomer system. Hence one should expect that the observed lamellar phase is indeed fluid, which is necessary for our model to be useful for real amphiphilic systems. To establish that this is true, we have studied the structure factor in the direction of, and perpendicular to, the director, plus the single particle dynamics in both directions.

The structure factor measured in the direction of the director should exhibit power-law singularities at $q = nq_0$, where $n = 1, 2, \dots$ and $q_0 = 2\pi/d$, where d is the layer spacing [34]: $S(q) \propto |q - nq_0|^{-2+n^2\eta}$, where $\eta > 0$ is non-universal and depends on the elastic constants. Figure 14, showing the $n = 1$ peak, exhibits this behavior quite nicely; the drawn curve is for $q_0 = 3.36$ (i. e. a layer spacing $d = 1.87$) and $\eta = 0$. The value of η for our system is rather small compared to two, and thus we found that our system size and statistical accuracy were insufficient to determine a meaningful number. Actually, the data are compatible with any value of η in the range $-0.3 \leq \eta \leq 0.2$. A rather small value of η is quite typical for analogous experimental systems [35]. The structure factor in the directions perpendicular to the director clearly shows fluid structure, as expected (see Fig. 15). Finally, the liquid crystalline behavior also clearly shows up in the anisotropy of the dynamics, see Fig. 16: While the in-plane diffusion (measured via the mean square displacement in the directions perpendicular to the director) is nearly unhindered, with quite similar behavior as in the liquid phase of the monomers, the inter-plane diffusion is strongly reduced, similar to the behavior in the monomer crystal. The resulting diffusion constants are listed in Table 2, where again the values for inter-plane diffusion are upper bounds only.

4 Conclusions and Outlook

We have introduced a new simple continuum simulation model for the investigation of amphiphilic and copolymeric systems. This model, or rather straightforward generalizations of it, is capable of reproducing many essential physical characteristics in the targeted area of interest. Compared to previous generic continuum models [13–16] our new model offers important technical advantages: All interactions are short ranged; therefore the number of interacting pairs is relatively small, resulting in good computational efficiency. We estimate this improvement to be roughly an order of magnitude. Furthermore, our approach of varying the strength of the attractive interaction as the temperature-like variable, while keeping kinetic energy and curvature of the potential constant, is ideally suited for MD, since a broad range of “temperatures” can be scanned without the need to use a smaller time step.

The structure of the monomeric fluid is hardly affected by the attractive tail compared to the purely repulsive Lennard-Jones fluid. The binary fluid of two disliking

components phase separates; this happens at an interaction strength which is roughly half the value of the interaction strength of the order–disorder transition, where the A–B dimeric liquid forms the liquid lamellar phase. We did not find any indication for any other ordered fluid phase for the dimer system. Both from structural analysis and from the observation of fast two–dimensional diffusion, we demonstrated that the lamellar phase is still fluid; crystallization occurs for stronger interactions. The diffusion constants of the pure fluid and the one within layers of dimers are of the same order of magnitude under same conditions. This establishes that the model at least satisfies the basic requirements.

The presented version is the most simple variant. Starting from there, one can generalize the model in a quite straightforward way, and connect not only two, but more monomers, as has been done previously [14,16], until one finally arrives at a model for a block copolymer. A great variety of molecular architectures is thus accessible. By this, one automatically includes the effects of tail length and of internal conformational entropy, which of course controls the effective interaction. How many and which intramolecular degrees of freedom should be included depends on the question under consideration, and is not obvious, since in part these may rather be incorporated by effective (usually density– and temperature dependent) potentials. This question is far from settled; within the framework of polymer simulations it is an active area of research [36]. As an example for such a generalized model, let us consider surfactants which consist of an A monomer, followed by four B monomers, and an A monomer again. In Fig. 17 we show a snapshot configuration of a system of such molecules diluted in an A solvent (not shown). A bicontinuous phase is stable at the simulated parameter values; however, we have not analyzed this systematically. This clearly shows that non–trivial configurations and phases are accessible to our simulation approach. It is also possible, within the framework of the present class of models, to devise a system where a single layer, arranged at the interface between A (“water”) and B (“oil”) solvent, would exhibit spontaneous curvature: This is simply achieved by making one of the types of monomers larger than the other one; note that the monomer “size” is controlled via the repulsive core of the interactions. Furthermore, bond bending potentials and torsional potentials can be introduced. Thus one can “dress” the model further and further, until one arrives at a description which is quite similar to a “united atom” model, at the expense of more and more complicated calculations. In particular, it is possible to construct “hard rods”, whose liquid–crystalline ordering is mainly driven by packing. Which kind of model is needed depends very much on the physical question under consideration; as a rule of thumb, more and more chemical detail will be needed the smaller the length scale under consideration is. For many interesting phenomena, atomistic simulations will remain indispensable. Our model, on the contrary, is expected to work best for collective phenomena which occur on large (mesoscopic or hydrodynamic) length and

time scales, like morphology formation of complex phases, shear alignment of lamellar structures, etc.

The authors thank the European Commission for support through TMR grant number ERB FMGE CT950051 (TRACS Program at Edinburgh Parallel Computer Center). Stimulating discussions with G. Auernhammer, H. R. Brand, H. Pleiner, and J. Vollmer are gratefully acknowledged.

References

1. W. M. Gelbart, A. Ben-Shaul, and D. Roux, *Micelles, Membranes, Microemulsions, and Monolayers* (Springer–Verlag, Berlin, 1994).
2. Y. Zhang, U. Wiesner, and H. W. Spiess, *Macromolecules* **27**, 5547 (1994).
3. H. Leist, D. Maring, T. Thurn–Albrecht, and U. Wiesner, *J. Chem. Phys.* **110**, 8225 (1999).
4. O. Diat, D. Roux, and F. Nallet, *J. Phys. II France* **3**, 1427 (1993).
5. D. Vollmer, R. Strey, and J. Vollmer, *J. Chem. Phys.* **107**, 3619 (1997).
6. J. Vollmer, D. Vollmer, and R. Strey, *J. Chem. Phys.* **107**, 3627 (1997).
7. J. Vollmer and D. Vollmer, *Farad. Discuss.* **112**, 51 (1999).
8. S. J. Marrink and A. E. Mark, *J. Phys. Chem. B* **105**, 6122 (2001).
9. J. C. Shelley, M. Y. Shelley, R. C. Reeder, S. Bandyopadhyay, and M. L. Klein, *J. Phys. Chem. B* **105**, 4464 (2001).
10. J. Eilhard, A. Zirkel, W. Tschöp, O. Hahn, K. Kremer, O. Schärpf, D. Richter, and U. Buchenau, *J. Chem. Phys.* **110**, 1819 (1999).
11. J. C. Wheeler and B. Widom, *J. Am. Chem. Soc.* **90**, 3064 (1968).
12. R. G. Larson, *J. Phys. II France* **6**, 1441 (1996).
13. R. Goetz and R. Lipowsky, *J. Chem. Phys.* **108**, 7397 (1998).
14. R. Goetz, G. Gompper, and R. Lipowsky, *Phys. Rev. Lett.* **82**, 221 (1999).
15. M. Laradji, O. G. Mouritsen, S. Toxvaerd, and M. J. Zuckermann, *Phys. Rev. E* **50**, 1243 (1994).
16. K. Esselink, P. A. J. Hilbers, N. M. van Os, B. Smit, and S. Karaborni, *Coll. Surf. A: Physicochem. Eng. Asp.* **91**, 155 (1994).
17. C. Loison, F. Schmid, and K. Kremer, in preparation.
18. Th. Soddemann, G. Auernhammer, H. R. Brand, H. Pleiner, and Kremer, in preparation.
19. M. P. Allen and D. J. Tildesley, *Computer Simulation of Liquids* (Clarendon, Oxford, 1987).
20. G. S. Grest and K. Kremer, *Phys. Rev. A* **33**, 3628 (1986).
21. K. Kremer and G. S. Grest, *J. Chem. Phys.* **92**, 5057 (1990).
22. G. S. Grest, M.–D. Lacasse, K. Kremer, and A. M. Gupta, *J. Chem. Phys.* **105**, 10583 (1996).
23. D. C. Rapaport, *The Art of Molecular Dynamics Simulation* (Cambridge University Press, New York, 1995).
24. B. Dünweg, G. S. Grest, and K. Kremer, in *Numerical Methods for Polymeric Systems*, edited by S. G. Whittington (Springer, Berlin, 1998), Vol. 102, p. 159.
25. A. Kolb and B. Dünweg, *J. Chem. Phys.* **111**, 4453 (1999).

26. M. Pütz and A. Kolb, *Comp. Phys. Comm.* **113**, 145 (1998).
27. N. Metropolis *et al.*, *J. Chem. Phys.* **21**, 335 (1953).
28. D. Frenkel, *Physica A* **263**, 26 (1999).
29. B. Dünweg, in *Monte Carlo and Molecular Dynamics of Condensed Matter Systems*, edited by K. Binder and G. Cicotti (Societa Italiana Fisica, Bologna, 1996), p. 215.
30. C. Kittel, *Introduction to Solid State Physics* (John Wiley & Sons, New York, 1995).
31. J.-P. Hansen and L. Verlet, *Phys. Rev.* **184**, 151 (1969).
32. A. M. Ferrenberg and D. P. Landau, *Phys. Rev. B* **44**, 5081 (1991).
33. P. G. de Gennes and J. Prost, *The Physics of Liquid Crystals* (Clarendon, Oxford, 1993).
34. P. M. Chaikin and T. C. Lubensky, *Principles of Condensed Matter Physics* (Cambridge University Press, Cambridge, 1995).
35. C. R. Safinya, D. Roux, G. S. Smith, S. K. Sinha, N. A. Clark, and A. M. Bellocq, *Phys. Rev. Lett.* **57**, 2718 (1986).
36. J. Baschnagel, K. Binder, P. Doruker, A. A. Gusev, O. Hahn, K. Kremer, W. L. Mattice, F. Müller-Plathe, M. Murat, W. Paul, S. Santos, U. W. Suter, and V. Tries, *Adv. Polym. Sci.* **152**, 41 (2000).

ϕ	1.4	1.5	1.7	1.9	2.4
D	$33.9 \cdot 10^{-3}$	$26.4 \cdot 10^{-3}$	$15.1 \cdot 10^{-3}$	$8.74 \cdot 10^{-3}$	$0.177 \cdot 10^{-3}$

Table 1. Pure fluid system diffusion constants for different values of the potential depth ϕ . The value for $\phi = 2.4$ must be considered as an upper bound.

ϕ	1.2	1.4	1.5
$D_{\text{in-plane}}$	$14.5 \cdot 10^{-3}$	$11.9 \cdot 10^{-3}$	$9.72 \cdot 10^{-3}$
$D_{\text{inter-plane}}$	$1.3 \cdot 10^{-3}$	$0.6 \cdot 10^{-3}$	$0.6 \cdot 10^{-3}$

Table 2. Diffusion constants for dimeric systems. $D_{\text{in-plane}}$ denotes the two-dimensional diffusion constants within a layer in the lamellar phase. $D_{\text{inter-plane}}$ represents the diffusion perpendicular to the layers. These latter values must be considered as upper bounds.

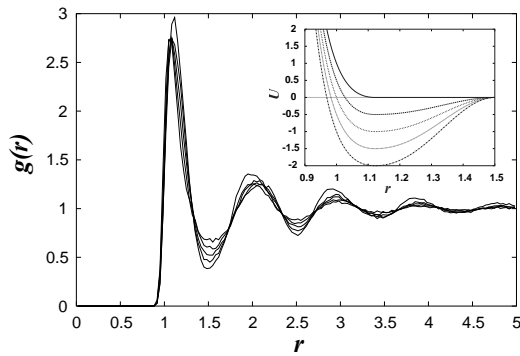


Fig. 1. Pair correlation function for different values of the potential depth $\phi = 0.0, 0.5, 1.0, 1.5, 2.0$. The curve with the largest oscillations refers to $\phi = 2.0$, the one with the smallest to $\phi = 0.0$, i. e. the purely repulsive Lennard–Jones fluid. The inset shows the corresponding potentials.

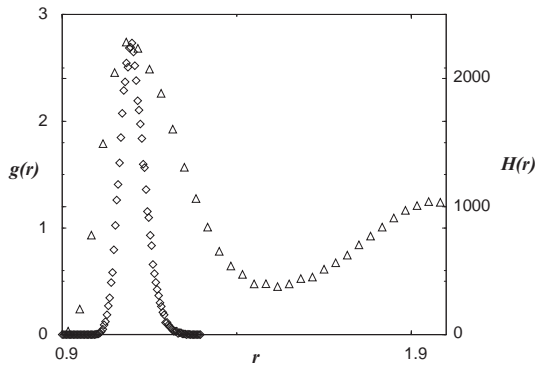


Fig. 2. Histogram of bond lengths for a system of dimers at $\rho = 0.85$, $\phi = 1.5$, compared to the pair correlation function $g(r)$ of a monatomic system at the same state point.

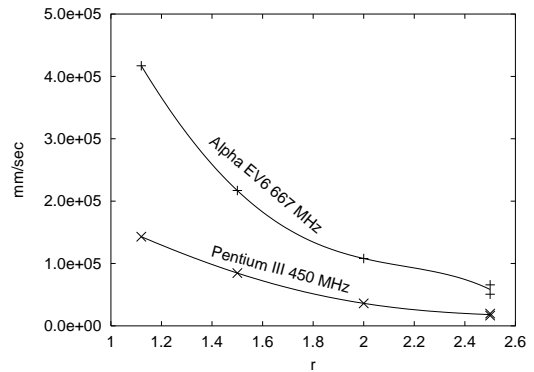


Fig. 3. Number of Molecular Dynamics steps per particle (“monomer moves”) per CPU second on two different hardware platforms as indicated in the figure. We study systems of pure monomers at density $\rho = 0.85$ with different ranges of interaction r : Purely repulsive LJ potential ($r = 2^{1/6}$), attractive cosine potential for $r = 1.5, 2.0, 2.5$, and standard LJ potential cut off at $r = 2.5$ (lower data points). The cosine potential was run at strength $\phi = 1.5$; the system size was always $N = 1000$ particles.

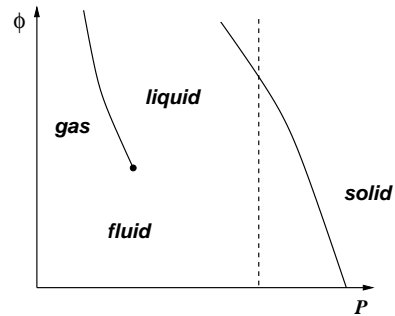


Fig. 4. Qualitative sketch of the expected phase diagram of a one-component system of monomers in the ϕ –pressure plane. The existence of the gas–liquid line was not proven numerically, but is strongly expected. All transition lines are of first order; the gas–liquid line ends in a critical point. Beyond this, there is only a “fluid” phase where there is no more a difference between gas and liquid. Furthermore, the diagram shows the path along which we studied the fluid–solid transition (dashed line).

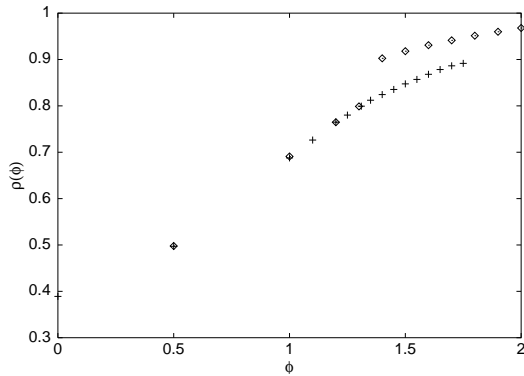


Fig. 5. Hysteresis loop of the density ρ as a function of the potential depth ϕ , at constant pressure $P = 1.0$, for $N = 10000$. The crosses denote the sweep of increasing ϕ , the diamonds decreasing ϕ .

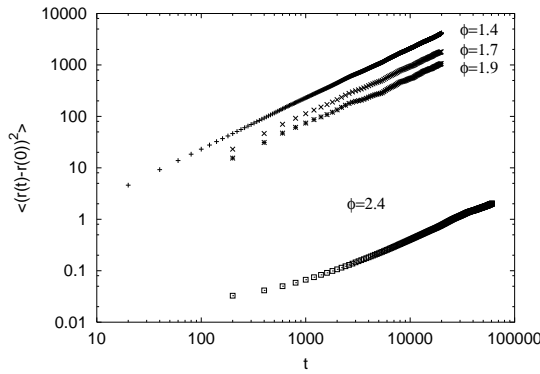


Fig. 6. Mean square displacement for different values of the potential depth ϕ .

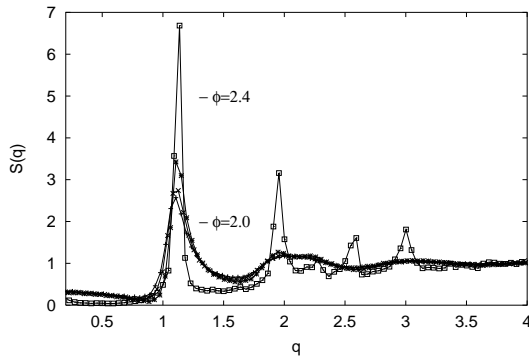


Fig. 7. Structure factor for systems with different values of the potential depth $\phi = 1.4$ (+), 1.8 (\times), 2.0 (\star) and 2.4 (\square). Configurations with $\phi \leq 2.0$ exhibit a fluid-like structure, while systems with higher values definitely show a crystal with fcc order.

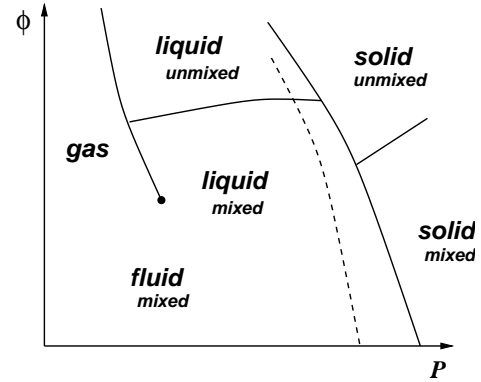


Fig. 8. Qualitative sketch of the expected phase diagram of a binary system of pure monomers in the ϕ -pressure plane, for fixed composition. The diagram is partly speculative even with respect to its topology. The transition line between the mixed and the unmixed state is of first order, except for the case of composition $1/2$ and liquid, where, due to the symmetry of the model, the transition is of second order. The dashed line denotes the path along which we have studied the unmixing transition (constant volume).

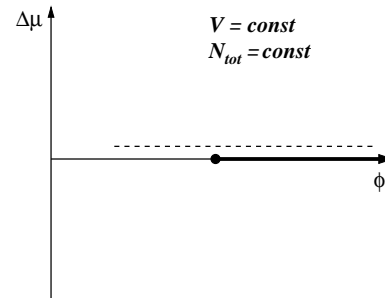


Fig. 9. Sketch of the unmixing phase diagram in the plane $(\phi, \Delta\mu)$, where $\Delta\mu$ is the chemical potential difference between species A and B. The first-order line occurs at $\Delta\mu = 0$, for reasons of A-B symmetry, and ends at an Ising-like critical point ϕ_c .

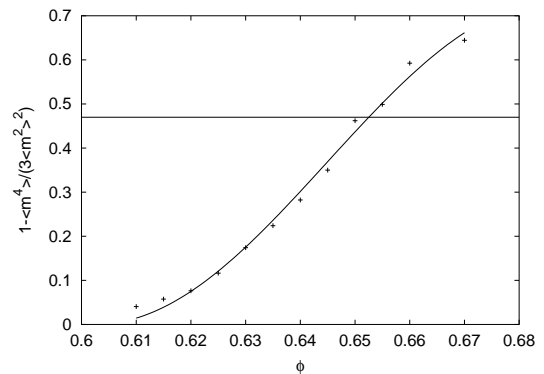


Fig. 10. Fourth order cumulant ratio for a binary system of $N = 4000$ particles in the semi-grandcanonical ensemble at density $\rho = 0.85$ as a function of ϕ . The horizontal line indicates the value 0.47 , which is the expected critical value for the 3d Ising universality class.

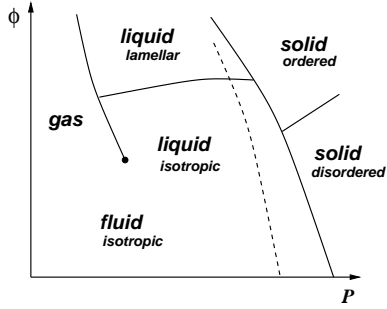


Fig. 11. Qualitative sketch of the expected phase diagram of a system of A-B dimers in the ϕ -pressure plane. Again, the diagram is partly speculative. The dashed line denotes the path along which we have studied the order-disorder transition (constant volume). All transition lines are of first order.

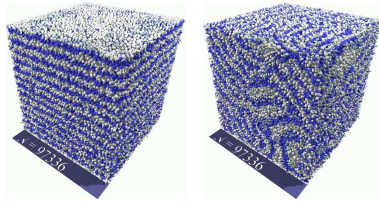


Fig. 12. Typical configurations for a potential depth of $\phi = 1.3$. The system is composed of 48668 A-B dimers at density $\rho = 0.85$. Left: Aligned lamellae, produced by proper sample preparation. Right: Lamellar domains, produced by quenching a disordered system into the ordered phase.

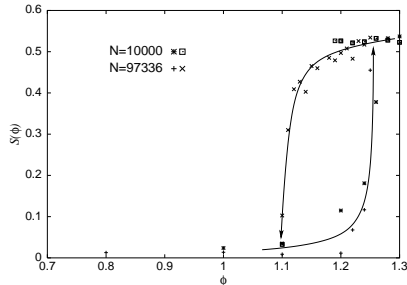


Fig. 13. Nematic order parameter S as a function of the potential depth ϕ . The plusses denote the way from $\phi = 0$ to larger ϕ for the system of $N = 97336$ particles, the crosses the reverse direction. The corresponding data for the $N = 10000$ system are represented by stars and boxes. The curves are drawn as guide to the eye.

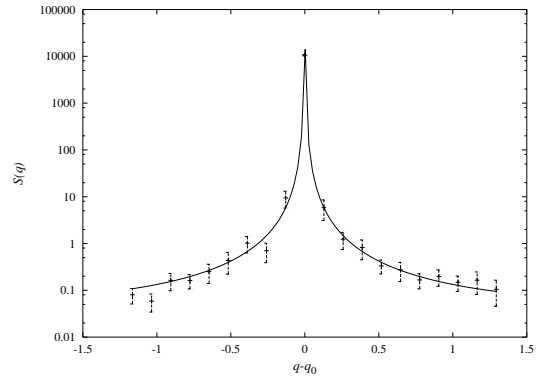


Fig. 14. Structure factor of a system of $N = 48668$ dimers at $\rho = 0.85$, $\phi = 1.3$ in the direction of the director, with $q_0 = 3.36$. Also shown is a curve $S(q) \propto |q - q_0|^{-2}$. In order to improve the statistics, the data include an average over wave vectors (q_x, q_y, q_z) , where z is the layer normal direction, and only a very small contribution in x and y direction was taken into account: $|q_x| \leq 0.01$, $|q_y| \leq 0.01$.

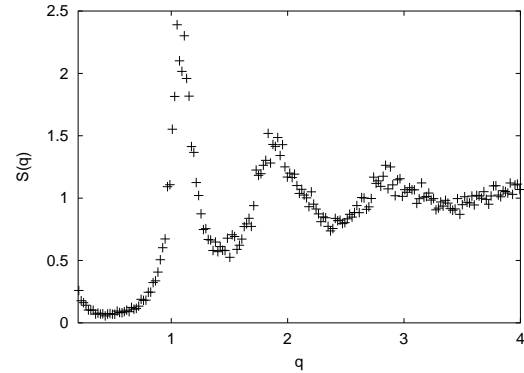


Fig. 15. Structure factor of a system of $N = 48668$ dimers at $\rho = 0.85$, $\phi = 1.3$ in the directions perpendicular to the director.

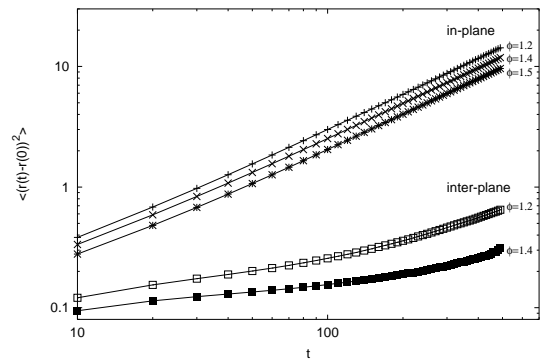


Fig. 16. Mean square displacements for different values of the potential depth ϕ , inter-plane and in-plane in comparison.

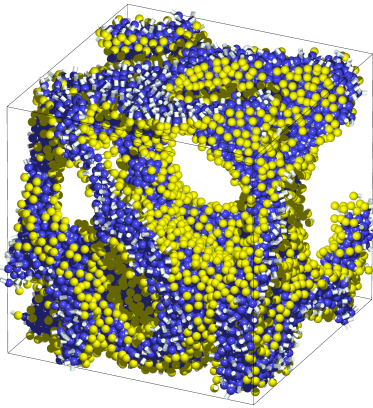


Fig. 17. Snapshot of a conformation in the bicontinuous phase of ABBBBA surfactants (see text), where A monomers are coded light and B monomers dark. Solvent particles (species A) are not shown. The surfactant concentration is close to 0.35 and the simulation was carried out at $\phi = 1.3$ with $N = 27000$ particles in total.